REVIEW

Recent advances in imaging crustal fault zones: a review

Hongfeng Yang

Abstract Crustal faults usually have a fault core and surrounding regions of brittle damage, forming a low-velocity zone (LVZ) in the immediate vicinity of the main slip interface. The LVZ may amplify ground motion, influence rupture propagation, and hold important information of earthquake physics. A number of geophysical and geodetic methods have been developed to derive high-resolution structure of the LVZ. Here, I review a few recent approaches, including ambient noise cross-correlation on dense across-fault arrays and GPS recordings of fault-zone trapped waves. Despite the past efforts, many questions concerning the LVZ structure remain unclear, such as the depth extent of the LVZ. High-quality data from larger and denser arrays and new seismic imaging technique using larger portion of recorded waveforms, which are currently under active development, may be able to better resolve the LVZ structure. In addition, effects of the along-strike segmentation and gradational velocity changes across the boundaries between the LVZ and the host rock on rupture propagation should be investigated by conducting comprehensive numerical experiments. Furthermore, high-quality active sources such as recently developed large-volume airgun arrays provide a powerful tool to continuously monitor temporal changes of fault-zone properties, and thus can advance our understanding of fault zone evolution.

Keywords Fault zone structure · Fault zone waves · Earthquake rupture · Temporal changes

H. Yang (✉)
Earth System Science Programme, The Chinese University of Hong Kong, Shatin, NT, Hong Kong
e-mail: hyang@cuhk.edu.hk

1 Introduction

A crustal fault is a fracture or a zone of fractures that separates different blocks of crust and accumulates aseismic strain subjected to large stress concentrations (e.g., Yang 2010). When the energy associated with the accumulated strain is suddenly released, an earthquake occurs on the fault and may cause severe ground shaking. Geological studies of faults exposed on the ground indicate that a fault is characterized as a narrow zone, termed "fault zone (FZ)" (e.g., Chester and Logan 1986; Chester et al. 1993). Since it is composed of highly fractured materials (e.g., Chester and Logan 1986; Schulz and Evans 1998, 2000; Sammis et al. 2009), the FZ is seismically recognized as a low-velocity zone (LVZ) with reduction in seismic velocities and elastic moduli relative to the host rocks. It has been suggested that the FZ structure holds critical keys of earthquake generation and physics (e.g., Scholz 1990; Kanamori 1994; Kanamori and Brodsky 2004). Furthermore, material properties of the FZ may also influence the migration of hydrocarbons and fluids, as well as the morphology of the land surface (e.g., Wibberley et al. 2008; Faulkner et al. 2010). High-resolution imaging of the FZ structure not only advances our understanding of earthquake physics and thus of better seismic hazard preparation and mitigation, but is also critical to evaluate the long-term deformation of crust.

Tremendous efforts have been made to obtain high-resolution images of FZ structure, including geological, geodetic, and geophysical approaches. However, many fundamental questions concerning the mechanics, structure, and evolution of FZ remain unclear. Recently, there have been a number of new approaches to infer the LVZ structure, e.g., ambient noise cross-correlation using a dense seismic array (Zhang and Gerstoft 2014; Hillers et al. 2014), modeling FZ trapped waves from high-rate GPS

data (Avallone et al. 2014), analysis of interseismic strain localization (Lindsey et al. 2014), and so on. In this paper, I review the results from a number of geophysical and geodetic techniques that were developed to image high-resolution fault zone structure. These techniques include gravity inversions, modeling Interferometric Synthetic Aperture Radar (InSAR) and GPS data, regional seismic tomography, FZ trapped waves, FZ head waves, FZ body waves, and ambient noise cross-correlation. Following these methods, I discuss the questions that remain open for debate and suggest a few research directions that may lead to a better understanding of the FZ structure and evolutions of crustal faults.

2 FZ properties and their effects

Direct measurements of the FZ properties are conducted on exhumed faults and by drilling active faults into seismogenic depths (e.g., Chester et al. 1993; Sieh et al. 1993; Johnson et al. 1994; Oshiman et al. 2001; Ma et al. 2006; Li et al. 2013b; Ujiie et al. 2013). The results have shown that the FZ includes a fault core that is usually a few centimeters to several meters in thickness (Fig. 1). Most of the tectonic deformation including coseismic slip is accommodated in the clay-rich fault core (e.g., Chester et al. 1993; Evans and Chester 1995). For example, the primary slip zone of the Flowers Pit Fault, a young normal fault located southwest of Klamath Falls, Oregon, has been found to be no more than 20 mm in width (Sagy and Brodsky 2009). Drilling across the Alpine fault, New Zealand, reveals a ~ 0.5-m-thick principal slip zone bounded by a 2-m-thick fault gouge (Sutherland et al. 2012). Furthermore, core samples recovered from the Japan Trench Fast Drilling Project (JFAST) that were conducted by the Integrated Ocean Drilling Program (IODP) following the 2011 M_W 9.0 Tohoku-Oki earthquake reveal a several-meter-thick pelagic clay layer where the plate-boundary faulting is suggested to occur (Ujiie et al. 2013).
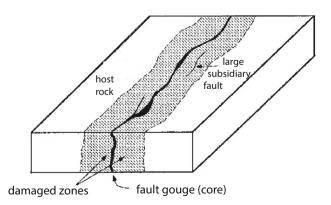

Fig. 1 A schematic plot of a typical fault zone, after Chester and Logan (1986)

In general, the size of the fault core is below the resolution of geophysical and geodetic imaging, and thus has to be analyzed by direct samples.

Surrounding the fault core is a damage zone that is usually composed of highly fractured materials, breccia, and pulverized rocks (e.g., Chester et al. 1993; Evans and Chester 1995). The damage zone, or the LVZ, often has a width of hundreds of meters to several kilometers (Fig. 1). For instance, analysis of core samples from the Yingxiu-Beichuan fault that ruptured in the devastating 2008 M_W 8.0 Wenchuan earthquake reveals a damage zone of approximate 100–200 m in width (Li et al. 2013b). Furthermore, fracture density has been found to drop drastically out of the central damage zones (100-m thick) along the Gole-Larghe Fault Zone in the Italian Alps (Smith et al. 2013) and the Flowers Pit Fault, Oregon (Sagy and Brodsky 2009).

The LVZ is often interpreted as a result of accumulative damages induced by past earthquakes. Therefore, the LVZ structure may reflect the behavior of past ruptures (e.g., Dor et al. 2006; Ben-Zion and Ampuero 2009; Xu et al. 2012). Furthermore, the LVZ can exert significant influence on properties of future ruptures based on results of numerical experiments (e.g., Harris and Day 1997; Huang and Ampuero 2011; Huang et al. 2014). For example, waves reflected from and propagated along the interfaces between the LVZ and intact rocks may strongly modulate the rupture propagation, including oscillations of rupture speed and generation of multiple slip pulses (Huang et al. 2014). In addition, the LVZ may result in amplification of ground motion near faults (e.g., Wu et al. 2009; Avallone et al. 2014; Kurzon et al. 2014) and may influence long-term deformation processes in the crust (e.g., Finzi et al. 2009; Kaneko et al. 2011). Moreover, cracks in the damage zone may store and transport fluids that play an important role on fault zone strength (Eberhart-Phillips et al. 1995). Due to closure of cracks and/or dry over wet cracks, seismic velocities in the LVZ may be elevated over time after a large earthquake. Such increase in seismic velocities of the LVZ indicates a healing process of the damage zone that is important to understand earthquake cycle and evolution of fault systems (Li et al. 1998; Vidale and Li 2003). Unfortunately, it is extremely difficult to determine FZ properties at seismogenic depths (McGuire and Ben-Zion 2005; Ben-Zion and Sammis 2009).

3 Techniques to image fault zones

A number of geophysical and geodetic techniques have been conducted to probe the FZ properties in depth. For example, using displacements captured by the InSAR data before and after an earthquake, low-velocity compliant zones have been discovered along the Calico, Rodman, and

Pinto Mountain faults, Southern California (Fialko et al. 2002). In addition, many geophysical methods have been applied in deriving FZ properties such as gravity and electromagnetic surveys, seismic reflection and refraction, travel-time tomography, earthquake location, waveform modeling of FZ-reflected body waves, FZ head waves, and FZ trapped waves (e.g., Mooney and Ginzburg 1986; Ben-Zion and Malin 1991; Ben-Zion et al. 1992; Hole et al. 2001; Prejean et al. 2002; Waldhauser and Ellsworth 2002; Li et al. 2002; McGuire and Ben-Zion 2005; Bleibinhaus et al. 2007; Li et al. 2007; Yang et al. 2009; Roland et al. 2012). In the following, I briefly review a few seismological and geodetic methods that have been used to derive FZ structure.

3.1 FZ waves

The most frequently used seismological technique to image FZ structure is to model the FZ trapped waves (FZTW), which are low frequency wave trains with relatively large amplitude following the S wave (e.g., Li et al. 1990). This method has been applied on different faults around the world, such as the North Anatolian fault zone in Turkey (Ben-Zion et al. 2003), the Nocera Umbra and San Demetrio faults in central Italy (Rovelli et al. 2002; Calderoni et al. 2012), the San Andreas fault (SAF) near Parkfield (Korneev et al. 2003; Li et al. 2004; Li and Malin 2008; Wu et al. 2010), the Lavic Lake fault zone (Li et al. 2003b), the Calico fault zone (Cochran et al. 2009), the Landers fault zone (Li et al. 1994, 1999, 2000; Peng et al. 2003), and the San Jacinto fault zone (SJFZ) in California (Li et al. 1997; Li and Vernon 2001; Lewis et al. 2005). Most FZTW studies have revealed a LVZ ranged from ~75 m to ~350 m in width with the shear wave velocity reduced by 20 %–50 % compared to the host rock. However, considerable uncertainties of FZTW modeling results due to the non-uniqueness and trade-off among FZ parameters have been noted (Peng et al. 2003; Lewis et al. 2005). Furthermore, it is still open for debate whether the trapping structure is shallow or deep (Li et al. 1997; Li and Vernon 2001; Ben-Zion and Sammis 2003; Lewis et al. 2005). For instance, a 15–20-km-deep LVZ of the SJFZ was reported by Li and Vernon (2001) while another group argued that it was only 3–5 km deep (Lewis et al. 2005). Recent FZTW studies using newly deployed dense linear arrays also reveal shallow damaged zones near the Jackass Flat across the SJFZ (Qiu et al. 2014).

In addition to the waves trapped within the LVZ, another type of wave that travels mostly along the fault interface, the so-called FZ head wave (FZHW), is also used to derive the FZ structure at depth. FZHWs are identified as low-amplitude and long-period precursory signals with polarities opposite to the direct P waves. The differential times between the FZHWs and direct P waves provide high-resolution information on the velocity contrast across the fault interface. For instance, measurements of such differential times and waveform modeling of head waves document 20 %–50 % of velocity contrast in the Bear Valley region of the SAF (McGuire and Ben-Zion 2005). Similarly, along-strike variation of velocity contrast along the Calaveras fault has also been suggested by modeling FZHW (Zhao and Peng 2008). In addition to inspecting waveforms directly, polarization analysis has been applied in automatically identifying FZHW (Allam et al. 2014b). By applying such automatic detection of FZHW and analysis of the differential times between the FZHW and direct P waves, average velocity contrasts of 3 %–8 % have been found along the Hayward fault, Northern California (Allam et al. 2014b). More recently, the FZHW has been observed along the Garzê-Yushu fault ruptured during the 2010 M_W 6.9 Yushu earthquake (Yang et al. 2015). This is by far the first observation of FZHWs along a non-major plate-boundary fault. Analysis of the time delays between the direct P waves and FZHWs suggests 5 %–8 % velocity contrast across the fault.

More recently, waveforms of body waves transmitted through the FZ and reflected from its boundaries have been used to derive the degree of damage, width, and depth extent of the LVZ (Fig. 2) (Li et al. 2007; Yang and Zhu 2010a; Yang et al. 2011, 2014). This technique not only uses measurements of travel-time delays of direct P and S waves, but also takes into account of the differential times between the direct and FZ-reflected P and S waves. Thus, the trade-off between the FZ width and the velocity reduction is largely removed (Li et al. 2007). Since the body waves are of higher frequencies than the FZTW, the body waves sampling the FZ may resolve the FZ structure in higher resolution. Another advantage of this method is that it allows us to trace individual seismic rays that travel through and bounce back multiple times from the FZ boundaries, as the synthetic travel times and waveforms are computed using the Generalized Ray Theory (GRT) (Helmberger 1983). In addition, this technique can well constrain the depth extent of the LVZ if it is combined with the waves that are diffracted from the base of the LVZ (Fig. 2b), and/or the cross-fault travel-time delays of first arrivals (Yang et al. 2011). For instance, the Buck Ridge branch of the SJFZ was suggested to host a 2-km deep LVZ based on waveform modeling of the FZ-diffracted waves (Yang and Zhu 2010a).

3.2 Ambient noise cross-correlation

In the past decade, ambient noise cross-correlation (ANCC) has been extensively used in imaging subsurface structures of regional and continental scales (Campillo and
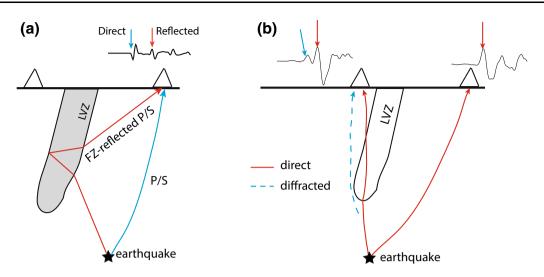
Fig. 2 Schematic plots for the direct and FZ-reflected P and S waves (**a**) and FZ-diffracted body waves (**b**). After Yang and Zhu (2010a)

Paul 2003; Shapiro et al. 2005; Yao et al. 2006). As recent data recordings from dense arrays become available, the ANCC technique has also been applied in higher frequency band to derive high-resolution crustal structure. For instance, by performing noise cross-correlation at a frequency band larger than 0.5 Hz, Zhang and Gerstoft (2014) have retrieved reliable Green's functions from long recordings (6 months) of ambient noise at a dense array across the Calico fault. The temporary array consists of 40 intermediate-period and 60 short-period (L22 2-Hz corner frequency) seismometers in a 1.5 km × 5.5 km grid adjacent to the Calico fault with minimum spacing of ∼50 m (Fig. 3). Similarly, FZ trapped waves were constructed from the scattered seismic wavefield recorded by the same array (Hillers et al. 2014). They also find the critical frequency of ∼0.5 Hz, a threshold above which the in-fault scattered wavefield has increased isotropy and coherency compared to the ambient noise (Hillers et al. 2014). The advantage of this approach is that the resolved structure is nearly independent on the background velocity model. The limitation of this technique, however, is that it can provide little constraint on the depth extent of the LVZ.

In addition to the Calico array, the ANCC technique has also been used on larger dense arrays. Between January and June 2011, a very dense seismic array was deployed in the Long Beach area as part of an active-source survey in petroleum industry (Lin et al. 2013; Schmandt and Clayton 2013). This array consists of more than 5200 high-frequency (10-Hz corner frequency) seismic velocity sensors within an area of 7–10 km, having a mean spacing of 120 m (Fig. 4a). As a by-product of the industry survey, the continuous recordings on the dense array provide unprecedented opportunities to image the subsurface structure at depths greater than petroleum reservoir. For instance,

clear fundamental-mode Rayleigh waves were observed from ambient noise tomography between 0.5 and 4 Hz, roughly corresponding to 1-km depth and above (Lin et al. 2013). A fast velocity anomaly was found beneath the active northwest–southeast trending Newport-Inglewood fault system that is covered by the Long Beach array. Whether this velocity anomaly is associated with the damage fault zone needs further investigations. In addition to deriving shallow crustal structures, data recorded at such a dense array can be used in illuminating deep crustal properties. For example, a sharp change in Moho depth was inferred from coherent lateral variations of travel times and amplitudes of P waves at frequencies near 1 Hz (Schmandt and Clayton 2013).

3.3 Gravity

Owing to a large number of fractures and possible fluid interaction and chemical alteration within the FZ, densities of the LVZs are significantly smaller than those of host rocks. Thus, the LVZ is usually associated with a negative Bouguer gravity anomaly so that its structure can be inferred from gravity data. From modeling Bouguer gravity data along the SJFZ, a 2–5 km wide damaged zone on both sides of the surface trace of the fault was proposed in the region (Stierman 1984). Similar results were reported along the Bear Valley section of the SAF (Wang et al. 1986). In addition, analysis of horizontal components of the Bouguer anomaly can clearly delineate a major plate-boundary fault, e.g., the Red River Fault in the South China Sea (Li et al. 2013a). Note that the gravity data is very valuable in deriving FZ structure in the ocean because seismic and other geodetic data are significantly limited. However, it is challenging to determine the fine structure and depth extent
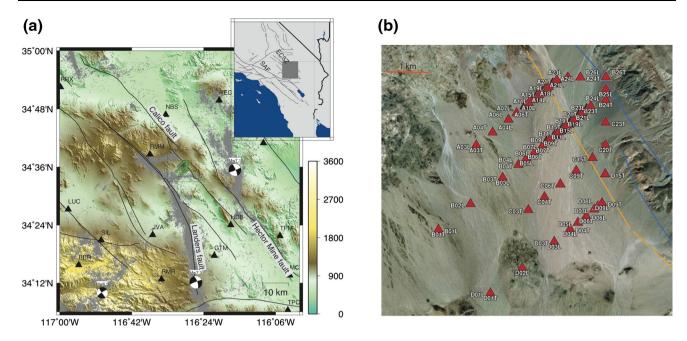
(a)

(b)

Fig. 3 **a** Map showing the Calico fault and nearby major earthquakes (beach balls), faults (*black lines*), and seismicity since 1981 (*gray crosses*). *Triangles* are the temporary array (*green*) deployed in 2006 and permanent stations (*black*) in the region. *Inset* figure is a map showing location of the Calico fault. *SAF* San Andreas Fault; *ECSZ* Eastern California Shear Zone. **b** *Red triangles* denote a temporary dense seismic array. Two segments of the Calico fault are shown near the array. *Orange* indicates Holocene faults and *blue* is Quaternary. After Yang et al. (2011)
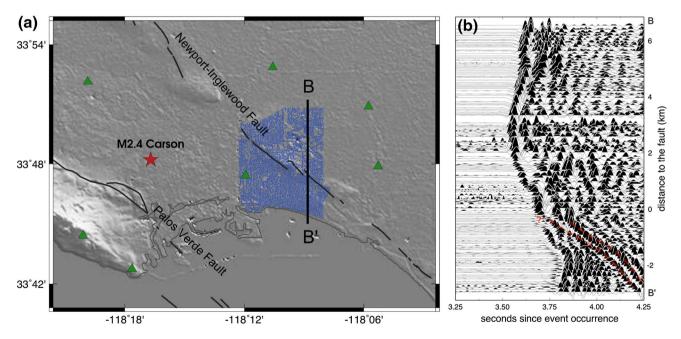
(a)

(b)

Fig. 4 **a** Locations of the long beach array (*blue dots*) and Southern California Seismic Network stations (*green triangles*). *Star* denotes a magnitude 2.4 earthquake whose waveforms are shown in *panel* (**b**). **b** P-wave waveform record section along a linear profile BB′ across the Newport-Inglewood fault

of the LVZ using gravity data alone due to nonuniqueness of the solution and relatively low resolution. Thus, application of gravity data to deriving FZ structure is considerably limited.

3.4 InSAR data

The aforementioned LVZ of the Calico fault was first discovered from InSAR data by comparing the ground

deformation before and after the neighboring 1999 M_W 7.1 Hector Mine earthquake (Fialko et al. 2002). Following this discovery, high-resolution satellite image data have been used to derive FZ structure, e.g., the Pinto Mountain fault and the Lenwood fault (Fialko 2004). It has also been pointed out that there might be considerable trade-off among the width, degree of damage (reduction in elastic moduli), and depth extent of the damage zone using the InSAR data (Barbot et al. 2009). Besides the coseismic deformation, interseismic strain derived from the InSAR data could also be used to determine the structure of the damaged FZ. For instance, the observed asymmetric patterns of interseismic deformation along the SAF and the SJFZ might be associated with kilometer-wide damage zones (Fialko 2006). However, such observations can be explained equally well by a model of a dipping fault zone (Fialko 2006). As such, application of the InSAR data to modeling FZ structure in depth should consider the nonuniqueness and trade-off among FZ parameters.

3.5 GPS data

In addition to modeling the InSAR data, deriving FZ structure from interseismic strain is also available by analysis of GPS data. Using a dislocation model in a heterogeneous elastic half space, Lindsey et al. (2014) have shown that a reduction in shear modulus within the FZ by a factor of 2.4 is required to fully explain the observed strain rate along the SJFZ, assuming a 15-km locking depth. Such reduction in elastic modulus and thus in seismic velocities is much higher than as imaged by regional seismic tomography (Allam and Ben-Zion 2012; Allam et al. 2014a). However, a similar magnitude of reduction in elastic modulus to the seismically determined value will result in a locking depth of 10 km, much shallower than the observed 14–18 km depth of seismicity along the SJFZ (Lindsey et al. 2014). Alternative possibility includes reduced yield strength within the upper FZ leading to the distributed plastic failure, as suggested by numerical modeling results (Duan 2010).

In addition to recording interseismic strain, high-rate GPS data may also record coseismic deformation. For instance, FZ trapped waves have been found, for the first time, at a 10-Hz sampling frequency GPS station near the April 6th, 2009, M_W 6.1 L'Aquila earthquake (Avallone et al. 2014). The GPS station was installed near L'Aquila a few days before the mainshock. The horizontal components of the mainshock waveforms contain a high-amplitude (43 cm peak-to-peak), nearly harmonic (1 Hz) wave train. Absence of this wave train in other nearby instrumental records indicates a local site effect, which is the wave energy trapped near the GPS station. The observation can be well fit by synthetic trapped waves in a model consisting of two quarter spaces separated by a 650-m wide LVZ that has 50 % velocity reduction and a Q value of 20 (Avallone et al. 2014).

4 Discussion

4.1 Depth extent of the LVZ

Despite the past efforts on imaging high-resolution FZ structure, many fundamental questions concerning the mechanics, structure, and evolution of FZ remain unclear. For example, a central debate of imaging FZ structure is to what depth the LVZ extends (Yang and Zhu 2010b). A number of studies suggest that the LVZ may extend to the base of seismogenic depth, such as the SJFZ (Li et al. 1997; Li and Vernon 2001), the SAF near Parkfield (Wu et al. 2010), and the San Demetrio Fault in central Italy (Calderoni et al. 2012). In stark contrast, a group of studies propose that the LVZ only extends to shallow depths, e.g., a few km below the surface. For example, it has been suggested that the SJFZ hosts LVZs extending to 2–5 km in depth according to modeling of LVZ trapped and diffracted waves (e.g., Lewis et al. 2005; Yang and Zhu 2010a). The LVZ of the Calico fault is also suggested to be no more than 3 km in depth (Yang et al. 2011).

Using a newly deployed dense seismic network, recent results of seismic imaging in regional scale have shown significant improvements in the resolution of crustal structure (e.g., Allam et al. 2014b; Zigone et al. 2014). Although the 100-m-wide LVZ is still below the current resolution of seismic images in regional scale, the newly obtained tomographic images of crustal velocity structure clearly show several-km-wide LVZs along the SJFZ, with strong velocity contrasts with host rocks (Allam et al. 2014b; Zigone et al. 2014). Furthermore, such LVZs are mostly prominent in the top 5 km, suggesting a shallow LVZ extent (Allam et al. 2014b; Zigone et al. 2014). The observed shallow LVZ structures are consistent with numerical simulation results on decreasing damage with depth (Ben-Zion and Shi 2005; Finzi et al. 2009; Kaneko and Fialko 2011).

Such shallow LVZ structure is also implied from laboratory experimental measurements on rock samples from an exhumed fault, the Gole-Larghe Fault Zone (GLFZ) in the Italian Southern Alps (Mitchell et al. 2013). The GLFZ is hosted in jointed crystalline basement and exposed across glacier-polished outcrops in the Italian Alps (Smith et al. 2013). Widespread occurrence of cataclasites associated with pseudotachylytes (solidified frictional melts) indicates ancient large earthquakes. Geochemical dating and analysis of the pseudotachylytes suggest that they were formed at 9–11 km depth, with ambient

temperatures of 250–300 °C. Using a combination of structural line transects and image analysis of samples collected across-fault strike, Smith et al. (2013) document a broadly symmetric across-strike damage structure of the GLFZ. The damage zone is distinguished by large variations in fracture density, distribution of pseudotachylytes, and microfracture sealing characteristics compared to the host rocks. The central damage zone is 100 m in width and is associated with highest fracture density. In addition to measuring the fracture density, Mitchell et al. (2013) have also measured acoustic P-wave velocities of the samples in laboratory. The results, however, show a higher P-wave velocity within the central damage zone than the surrounding alteration zones that have smaller fracture density. Why isn't the central damage zone a LVZ? The interpretation is that a large number of cracks within the central damage zone were associated with pervasive sealing of fractures at depth, which is consistent with low permeability as measured in samples (Mitchell et al. 2013). Therefore, the seismic wave velocities in the FZ may not be lower than those in the host rocks. Considering that the samples were exhumed from ∼10 km in depth, the results imply that the FZ damage may have been generated at greater depth following large earthquakes but may have healed rapidly due to fluid-rock interaction.

4.2 FZ healing

Healing process is an important component in understanding earthquake cycle and long-term evolution of fault systems (e.g., Li et al. 1998; Vidale and Li 2003). It has been pointed out that a FZ, at least the shallow portion, may experience an increase in seismic velocity with time, indicating the healing of the damage zone after a large earthquake (Li et al. 1998, 2003a). By conducting a pair of seismic explosions and analysis of travel-time changes of identical shot-receiver pairs across the Johnson Valley fault ruptured in the 1992 Landers earthquake, Li et al. (1998) have found a ∼1 % increase in both P-wave and S-wave velocities from 1994 to 1996. Such velocity increase is consistent with the prevalence of dry over wet cracks and/ or the closure of dry cracks (Li et al. 1998). Similar to the observations along the Landers rupture zone, the fault zones ruptured during the 1999 Hector Mine M_W 7.1 earthquake have experienced a strengthening process during which the P-wave and S-wave velocities of FZ rocks increased by ∼0.7 %–1.4 % and ∼0.5 %–1.0 % between 2000 and 2001, respectively (Li et al. 2003a).

To accurately document the degree of FZ healing in the field, repeatable seismic sources such as repeating earthquakes and explosions are often used. However, even repeating earthquakes identified from waveform correlations and man-made explosions may not provide perfect repeatable sources, which may lead to considerable uncertainties in estimating the relatively small changes in velocity over time. Moreover, the episodic behavior of such natural and anthropogenic seismic sources prevents continuous monitoring of the temporal changes of subsurface structures. The ANCC method, in comparison, is independent of seismic sources and can provide continuous measurement of temporal changes of medium properties (e.g., Brenguier et al. 2008). For example, more than 5 years of ambient noise data have been used to derive the velocity changes over time at the SAF near Parkfield. The results illustrate the coseismic damages due to the M 6.5 San Simeon and the M 6.0 Parkfield earthquakes and the consequent healing, i.e., increase in velocity (Brenguier et al. 2008).

Many observations have been reported on temporal velocity changes in fault zones and volcanic areas from the ANCC results (e.g., Chen et al. 2014; Liu et al. 2014). However, the resolution of the ANCC results is often limited by the frequency of extracted signals. Recently, a new artificial seismic source has been implemented in probing high-resolution temporal changes of crustal velocities, termed transmitting seismic station (TSS) (Wang et al. 2012). The TSS is heavy-duty, easily controllable, and environmentally friendly. Its core part is an air-gun array that can suddenly release large-volume compressed air in a short-time interval, making highly repeatable (if not completely identical) seismic signals with cross-correlation coefficients larger than 0.99. The signals can be clearly observed at seismic stations over distances of ∼300 km after stacking, showing clear crustal phases (Fig. 5). Therefore, the TSS can not only be used to investigate FZ healing but also can provide valuable information of temporal structural changes over a larger scale. The TSS is currently under active development in China. After it was first launched in Binchuan, Yunnan, in April 2011 (Wang et al. 2012), another three test sites have been constructed in Xinjiang, Fujian, and Gansu provinces. Figure 5 shows the location of the TSS in Xinjiang and an example of the stacked waveforms excited from the air-gun source.

4.3 LVZ boundaries

It has been documented that the FZ damage may remain throughout (and beyond) earthquake cycles (Cochran et al. 2009; Yang et al. 2014). For instance, a 1.5-km-wide LVZ of the Calico fault has been suggested to be the long-lived damage zone given that there were no significant earthquakes along the Calico fault in the past thousands of years (Cochran et al. 2009; Yang et al. 2011). A more recent study also points out that the prominent LVZ near the Anza seismic gap along the SJFZ indicates slow healing process at least at shallow depths (Yang et al. 2014), as the Anza
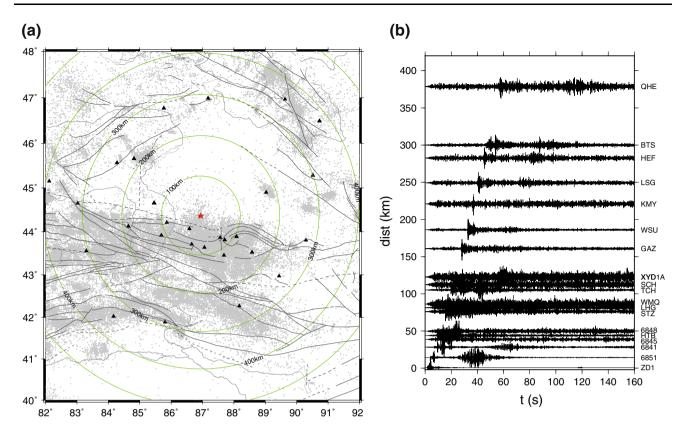
Fig. 5 **a** Locations of the air-gun source (*red star*) and permanent seismic stations (*black triangles*) in Xinjiang, China. *Gray circles* indicate seismicity from 1970 to 2013. *Blue lines* are fault traces. Large *green circles* denote the distance from the source. **b** Waveform cross section (vertical component) recorded by permanent stations. Waveforms are stacked for 100 air-gun shots. Station names are labeled at the right side of each trace. After Wang et al. (2013)

seismic gap has not experienced any surface-rupturing earthquakes for at least 200 years (Salisbury et al. 2012). Such healing process may be due to the closure of open cracks and fluid-sealing of fractures, which may in turn lead to less sharp boundaries between the LVZ and the host rock. Whether the velocity contrast occurs in a gradual transition zone or along a sharp interface may strongly affect the rupture properties of earthquakes on the fault and the FZ-related waveforms, e.g., the FZ-reflected waves.

Prominent FZ-reflected P and S waves were first observed at a linear array across the Landers fault that was deployed shortly after the 1992 M_W 7.3 Landers earthquake (Li et al. 2007). In contrast, such clear FZ-reflected phases are not identified coherently on the cross-fault arrays along the SJFZ and the Calico fault (Yang and Zhu 2010a; Yang et al. 2011, 2014). The difference may reflect the boundary properties between the FZ and the host rock. Since the array across the Landers fault was deployed shortly after the 1992 M_W 7.3 earthquake, the earthquake-induced damage may have generated strong velocity contrast between the damage zone and the host rock, forming sharp boundaries that can generate clear FZ-reflected waves. In

contrast, the SJFZ and the Calico fault have not experienced major ruptures in over 100 and 1000 years, respectively. Therefore, the LVZ boundaries might be gradual, resulting in less prominent reflected phases. Such gradual changes in FZ materials are observed by drilling into seismogenic faults. For example, a ∼50-m-thick alteration zone was found to obscure the boundary between the damage zone and fault core across the Alpine fault, New Zealand (Sutherland et al. 2012).

4.4 Effects of the FZ properties on dynamic ruptures

It has been well documented that the LVZ structure may strongly affect the dynamic rupture process (Harris and Day 1997; Huang and Ampuero 2011; Huang et al. 2014). Results of recent numerical simulations have shown the impacts on the rise time of slip and the transition from pulse-like to crack-like rupture as the LVZ width increases (Huang and Ampuero 2011). Considering large variations in width of damage fault zones (Savage and Brodsky 2011), e.g., the faults in the Eastern California Shear Zone, rupture propagation pattern for earthquakes occurring on

the Calico fault (1.5-km-wide LVZ) may be significantly different compared to the Landers (350-m-wide LVZ) and Hector Mine (100-m-wide LVZ) earthquakes.

The present numerical simulations of effects of LVZ on rupture dynamics are mostly conducted in 2-D cases with simplified LVZ structures. Many features in FZ structures revealed from observations are reasonably ignored. As mentioned above, there may be a transition zone between the damage zone and the host rock. Effects of such gradual changes in seismic velocity and elastic properties on rupture nucleation, propagation, and arrest are not well understood yet. Moreover, it has been pointed out that there are along-strike segmentations of the LVZ, as suggested along the SJFZ (Yang et al. 2014) and the SAF near Parkfield (Lewis and Ben-Zion 2010). Whether and how the segmented LVZs affect future earthquake ruptures needs to be investigated through numerical experiments. Furthermore, it has been shown that geometrically complex and heterogeneous fault properties also play important roles in dynamic rupture process (e.g., Yang et al. 2012, 2013). When coupled with the complex structure of the LVZ, which is likely the case in field, factors influencing rupture nucleation and propagation need to be investigated by conducting comprehensive numerical simulations.

5 Conclusions and future directions

Tremendous efforts have been conducted in imaging FZ structure and investigating FZ evolution and effects of FZ on rupture dynamics. In this paper, I briefly review the recent advances that have been used in deriving high-resolution images of the FZ structure, including seismological and geodetic approaches. The available active source, dense array deployment, as well as the more advanced computational resources, lay out the road to obtain better images of the FZ structure and to advance our understanding of the FZ evolution, earthquake initiation, rupture propagation, and termination on the fault.

Based on what are reviewed above, I think much can be learned by pursuing research in the following directions:

(1) Deployment of large dense arrays. There are numerous examples showing the power of seismic arrays in deriving better images of the Earth structure. It also holds true for the relatively small structure such as a FZ. For example, the Long Beach array provides an unprecedented opportunity to study high-resolution FZ structure using a variety of techniques. Figure 4b shows a waveform record section along a linear profile of the array in which a number of coherent FZ-related phases can be identified, and then modeled to obtain a much-detailed FZ structure. Not only

providing higher-quality data, the dense arrays will also promote development of new techniques in seismic imaging.

(2) Development of new imaging techniques. So far modeling of FZ waves is mostly focused on separated seismic phases, such as FZ-reflected body waves, FZHW, and FZTW. By using a larger portion of the recorded seismic wavefield, we should be able to better resolve the FZ structure to which the different waves are sensitive. As more advanced computational resources are available, wavefield-based seismic imaging technique such as adjoint tomography can be applied in deriving high-resolution images of FZ structure.

(3) Monitoring FZ evolution. As the highly repeatable seismic sources can be routinely used (Wang et al. 2012), continuously monitoring high-resolution FZ properties becomes feasible given that a dense seismic network is deployed across a FZ. With such a dense array and the high-quality active source, we can derive the high-resolution temporal variations of FZ structure and better understand how a FZ evolves with time.

References

Allam AA, Ben-Zion Y (2012) Seismic velocity structures in the southern California plate-boundary environment from double-difference tomography. Geophys J Int 190:1181–1196. doi:10.1111/j.1365-246X.2012.05544.x

Allam AA, Ben-Zion Y, Kurzon I, Vernon F (2014a) Seismic velocity structure in the Hot Springs and trifurcation areas of the San Jacinto Fault Zone, California, from double-difference tomography. Geophys J Int 198(2):978–999. doi:10.1093/gji/ggu176

Allam AA, Ben-Zion Y, Peng Z (2014b) Seismic imaging of a bimaterial interface along the Hayward Fault, CA, with fault zone head waves and direct P arrivals. Pure appl Geophys 171:2993–3011. doi:10.1007/s00024-014-0784-0

Avallone A, Rovelli A, Giulio GD, Improta L, Ben-Zion Y, Milana G, Cara F (2014) Wave-guide effects in very high rate GPS record

of the 6 April 2009, M_W 6.1 L'Aquila, central Italy earthquake. J Geophys Res. doi:10.1002/2013JB010475

Barbot S, Fialko Y, Sandwell D (2009) Three-dimensional models of elastostatic deformation in heterogeneous media, with applications to the Eastern California Shear Zone. Geophys J Int 179:500–520. doi:10.1111/j.1365-246X.2009.04194.x

Ben-Zion Y, Ampuero J-P (2009) Seismic radiation from regions sustaining material damage. Geophys J Int 178(3):1351–1356. doi:10.1111/j.1365-246X.2009.04285.x

Ben-Zion Y, Malin P (1991) San Andreas fault zone head wave near Parkfield, California. Science 251:1592–1594

Ben-Zion Y, Sammis CG (2003) Characterization of fault zones. Pure appl Geophys 160:677–715

Ben-Zion Y, Sammis C (2009) Mechanics, structure and evolution of fault zones. Pure appl Geophys 166:1533–1536. doi:10.1007/s00024-009-0509-y

Ben-Zion Y, Shi Z (2005) Dynamic rupture on a material interface with spontaneous generation of plastic strain in the bulk. Earth Planet Sci Lett 236:486–496. doi:10.1016/j.epsl.2005.03.025

Ben-Zion Y, Katz S, Leary P (1992) Joint inversion of fault zone head waves and direct P arrivals for crustal structure near major faults. J Geophys Res 97:1943–1951

Ben-Zion Y, Peng Z, Okaya D, Seeber L, Armbruster JG, Ozer N, Michael J, Baris S, Aktar M (2003) A shallow fault-zone structure illuminated by trapped waves in the Karadere-Duzce branch of the North Anatolian fault, western Turkey. Geophys J Int 152(3):699–717. doi:10.1046/j.1365-246X.2003.01870.x

Bleibinhaus F, Hole JA, Ryberg T, Fuis GS (2007) Structure of the California Coast Ranges and San Andreas fault at SAFOD from seismic waveform inversion and reflection imaging. J Geophys Res. doi:10.1029/2006JB004611

Brenguier F, Campillo M, Hadziioannou C, Shapiro NM, Nadeau RM, Larose E (2008) Postseismic relaxation along the San Andreas Fault at Parkfield from continuous seismological observations. Science 321:1478–1481. doi:10.1126/science.1160943

Calderoni G, Giovambattista RD, Vannoli P, Pucillo S, Rovelli A (2012) Fault-trapped waves depict continuity of the fault system responsible for the 6 April 2009 M_W 6.3 L'Aquila earthquake, central Italy. Earth Planet Sci Lett 323:1–8. doi:10.1016/j.epsl.2012.01.003

Campillo M, Paul A (2003) Long-range correlations in the diffuse seismic coda. Science 299:547–549. doi:10.1126/science.1078551

Chen H, Ge H, Niu F (2014) Semiannual velocity variations around the 2008 M_W 7.9 Wenchuan Earthquake fault zone revealed by ambient noise and ACROSS active source data. Earthq Sci 27:529–540. doi:10.1007/s11589-014-0089-5

Chester FM, Logan JM (1986) Implications for mechanical properties of brittle faults from observations of the Punchbowl Fault zone, California. Pure appl Geophys 124:79–106

Chester FM, Evans JP, Biegel RL (1993) Internal structure and weakening mechanisms of the San Andreas fault. J Geophys Res 98:771–786

Cochran ES, Li Y, Shearer PM, Barbot S, Fialko Y, Vidale JE (2009) Seismic and geodetic evidence for extensive, long-lived fault damage zones. Geology 37:315–318. doi:10.1130/G25306A.1

Dor O, Rockwell TK, Ben-Zion Y (2006) Geological observations of damage asymmetry in the structure of San Jacinto, San Andreas and Punchbowl faults in southern California: a possible indicator for preferred rupture propagation direction. Pure appl Geophys 163:301–349

Duan B (2010) Inelastic response of compliant fault zones to nearby earthquakes. Geophys Res Lett. doi:10.1029/2010GL044150

Eberhart-Phillips D, Stanley WD, Rodriguez BD, Lutter WJ (1995) Surface seismic and electrical methods to detect fluids related to faulting. J Geophys Res 97:12919–12936

Evans JP, Chester FM (1995) Fluid-rock interaction in faults of the San Andreas system: inferences from San Gabriel fault rock geochemistry and microstructures. J Geophys Res 100(B7):13007–13020

Faulkner DR, Jackson CAL, Lunn RJ, Schlische RW, Shipton ZK, Wibberley CAJ, Withjack MO (2010) A review of recent developments concerning the structure, mechanics and fluid flow properties of fault zones. J Struct Geol 32:1557–1575. doi:10.1016/j.jsg.2010.06.009

Fialko Y (2004) Probing the mechanical properties of seismically active crust with space geodesy: study of the coseismic deformation due to the 1992 M_W 7.3 Landers (southern California) earthquake. J Geophys Res 109:983–988. doi:10.1029/2003JB002756

Fialko Y (2006) Interseismic strain accumulation and the earthquake potential on the southern San Andreas fault system. Nature 441:968–971. doi:10.1038/nature04797

Fialko Y, Sandwell D, Agnew D, Simons M, Shearer P, Minster B (2002) Deformation on nearby faults induced by the 1999 Hector Mine earthquake. Science 297:1858–1862. doi:10.1126/science.1074671

Finzi Y, Hearn EH, Ben-Zion Y, Lyakhovsky V (2009) Structural properties and deformation patterns of evolving strike-slip faults: numerical simulations incorporating damage rheology. Pure appl Geophys 166:1537–1573. doi:10.1007/s00024-009-0522-1

Harris RA, Day SM (1997) Effects of a low-velocity zone on a dynamic rupture. Bull Seismol Soc Am 87:1267–1280

Helmberger DV (1983) Theory and application of synthetic seismograms. In: Kanamori H (ed) Earthquakes: observation, theory and interpretation, pp 174–222, Soc. Italiana di Fisica, Bologna

Hillers G, Campillo M, Ben-Zion Y, Roux P (2014) Seismic fault zone trapped noise. J Geophys Res. doi:10.1002/2014JB011217

Hole JA, Catchings RD, Clair KCS, Rymer MJ, Okaya DA, Carney BJ (2001) Steep-dip seismic imaging of the shallow San Andreas Fault near Parkfield. Science 294:1513–1515

Huang Y, Ampuero JP (2011) Pulse-like ruptures induced by low-velocity fault zones. J Geophys Res. doi:10.1029/2011JB008684

Huang Y, Ampuero J, Helmberger DV (2014) Earthquake ruptures modulated by waves in damaged fault zones. J Geophys Res. doi:10.1002/2013JB010724

Johnson AM, Fleming RW, Cruikshank KM (1994) Shear zones formed along long, straight traces of fault zones during the 28 June 1992 Landers, California earthquake. Bull Seismol Soc Am 84:499–510

Kanamori H (1994) Mechanics of earthquakes. Ann Rev Earth Planet Sci 22:207–237

Kanamori H, Brodsky EE (2004) The physics of earthquakes. Rep Prog Phys 67:1429–1496

Kaneko Y, Fialko Y (2011) Shallow slip deficit due to large strike-slip earthquakes in dynamic rupture simulations with elasto-plastic off-fault response. Geophys J Int 186:1389–1403

Kaneko Y, Ampuero JP, Lapusta N (2011) Spectral-element simulations of long-term fault slip: effect of low-rigidity layers on earthquake-cycle dynamics. J Geophys Res. doi:10.1029/2011JB008395

Korneev VA, Nadeau RM, McEvilly TV (2003) Seismological studies at Parkfield IX: fault-zone imaging using guided wave attenuation. Bull Seismol Soc Am 93:1415–1426

Kurzon I, Vernon F, Ben-Zion Y, Atkinson G (2014) Ground motion prediction equations in the San Jacinto Fault Zone—significant effects of rupture directivity and fault zone amplification. Pure appl Geophys. doi:10.1007/s00024-014-0855-2

Lewis M, Ben-Zion Y (2010) Diversity of fault zone damage and trapping structures in the Parkfield section of the San Andreas Fault from comprehensive analysis of near fault seismograms.

Geophys J Int 183:1579–1595. doi:10.1111/j.1365-246X.2010.04816.x

Lewis MA, Peng ZG, Ben-Zion Y, Vernon FL (2005) Shallow seismic trapping structure in the San Jacinto fault zone near Anza, California. Geophys J Int 162:867–881. doi:10.1111/j.1365-246X.2005.02684.x

Li Y, Malin PE (2008) San Andreas Fault damage at SAFOD viewed with fault-guided waves. Geophys Res Lett. doi:10.1029/2007GL032924

Li YG, Vernon FL (2001) Characterization of the San Jacinto fault zone near Anza, California, by fault zone trapped waves. J Geophys Res 106:30671–30688

Li YG, Leary PG, Aki K, Malin P (1990) Seismic trapped modes in the Oroville and San Andreas fault zones. Science 249:763–766

Li YG, Aki K, Adams D, Hasemi A, Lee WHK (1994) Seismic guided waves trapped in the fault zone of the Landers, California, earthquake of 1992. J Geophys Res 99:11705–11722

Li YG, Vernon FL, Aki K (1997) San Jacinto fault-zone guided waves: a discrimination for recently active fault strands near Anza, California. J Geophys Res 102:11689–11701

Li YG, Vidale JE, Aki K, Xu F, Burdette T (1998) Evidence of shallow fault zone strengthening after the 1992 M 7.5 Landers, California, earthquake. Science 279:217–219

Li YG, Vidale JE, Aki K, Xu F (1999) Shallow structure of the Landers fault zone from explosion-generated trapped waves. J Geophys Res 104:20257–20275

Li YG, Vidale JE, Aki K, Xu F (2000) Depth-dependent structure of the Landers fault zone using fault zone trapped waves generated by aftershocks. J Geophys Res 105:6237–6254

Li YG, Vidale JE, Day SM, Oglesby DD, SCEC Field Working Team (2002) Study of the 1999 M 7.1 Hector Mine, California, earthquake fault plane by trapped waves. Bull Seismol Soc Am 92:1318–1332

Li Y, Vidale JE, Day SM, Oglesby DD, Cochran E (2003a) Postseismic fault healing on the rupture zone of the 1999 m 7.1 Hector Mine, California, Earthquake. Bull Seismol Soc Am 93(2):854–869. doi:10.1785/0120020131

Li YG, Vidale JE, Oglesby DD, Day SM, Cochran E (2003b) Multiple-fault rupture of the M 7.1 Hector Mine, California, earthquake from fault zone trapped waves. J Geophys Res 108(B3): 2165. doi:10.1029/2001JB001456

Li YG, Vidale JE, Cochran ES (2004) Low-velocity damaged structure of the San Andreas Fault at Parkfield from fault zone trapped waves. Geophys Res Lett. doi:10.1029/2003GL019

Li H, Zhu L, Yang H (2007) High-resolution structures of the Landers fault zone inferred from aftershock waveform data. Geophys J Int 171:1295–1307. doi:10.1111/j.1365-246X.2007.03608.x

Li F, Sun Z, Yang H (2013a) Reconstruction of the mesozoic subduction in the South China Sea and its implications on the opening of the South China Sea basins. Eos Trans AGU, Fall Meet. Suppl OS21B-1624

Li H, Wang H, Xu Z, Si J, Pei J, Li T, Huang Y, Song SR, Kuo LW, Sun Z, Chevalier M-L, Liu D (2013b) Characteristics of the fault-related rocks, fault zones and the principal slip zone in the Wenchuan Earthquake Fault Scientific Drilling Project Hole-1 (WFSD-1). Tectonophysics 584:23–42. doi:10.1016/j.tecto.2012.08.021

Lin F, Li D, Clayton RW, Hollis D (2013) High-resolution 3D shallow crustal structure in Long Beach, California: application of ambient noise tomography on a dense seismic array. Geophysics 78:Q45–Q56. doi:10.1190/GEO2012-0453.1

Lindsey EO, Sahakian VJ, Fialko Y, Bock Y, Barbot S, Rockwell TK (2014) Interseismic strain localization in the San Jacinto fault zone. Pure appl Geophys 171(11):2937–2954. doi:10.1007/s00024-013-0753-z

Liu Z, Huang J, Peng Z, Su J (2014) Seismic velocity changes in the epicentral region of the 2008 Wenchuan earthquake measured from three-component ambient noise correlation techniques. Geophys Res Lett 41:37–42. doi:10.1002/2013GL058682

Ma K et al (2006) Slip zone and energetics of a large earthquake from the Taiwan Chelungpu-fault Drilling Project. Nature 444: 473–476

McGuire J, Ben-Zion Y (2005) High-resolution imaging of the Bear Valley section of the San Andreas fault at seismogenic depths with fault-zone head waves and relocated seismicity. Geophys J Int 163:152–164. doi:10.1111/j.1365-246X.2005.02703.x

Mitchell T, Rempe M, Smith S, Renner J, Toro GD (2013) Damage, permeability and sealing processes of an exhumed seismic fault zone: the Gole-Larghe Fault Zone, Italian Alps, EGU General Assembly, Vienna, p 13026

Mooney WD, Ginzburg A (1986) Seismic measurements of the internal properties of fault zones. Pure appl Geophys 124: 141–157

Oshiman N, Shimamoto T, Takemura K, Wibberley CAJ (2001) Thematic issue: Nojima fault zone probe, Island Arc, pp 195–505

Peng Z, Ben-Zion Y, Michael AJ, Zhu LP (2003) Quantitative analysis of seismic fault zone waves in the rupture zone of the Landers, 1992, California earthquake: evidence for a shallow trapping structure. Geophys J Int 155:1021–1041

Prejean S, Ellsworth W, Zoback M, Waldhauser F (2002) Fault structure and kinematics of the Long Valley Caldera region, California, revealed by high-accuracy earthquake hypocenters and focal mechanism stress inversions. J Geophys Res 107:2355. doi:10.1029/2001JB001,168

Qiu H, Ben-Zion Y, Ross ZE, Share P-E, Vernon F (2014) Internal structure of the San Jacinto fault zone at Jackass Flat from data recorded by a dense linear array, the SCEC annual meeting, SCEC, Palm Springs. Accessed 09 July 2014

Roland E, Lizarralde D, McGuire JJ, Collins JA (2012) Seismic velocity constraints on the material properties that control earthquake behavior at the Quebrada-Discovery-Gofar transform faults, East Pacific Rise. J Geophys Res. doi:10.1029/2012JB009422

Rovelli A, Caserta A, Marra F, Ruggiero V (2002) Can seismic waves be trapped inside an inactive fault zone? The case study of Nocera Umbra, central Italy. Bull Seismol Soc Am 92: 2217–2232

Sagy A, Brodsky E (2009) Geometric and rheological asperities in an exposed fault zone. J Geophys Res. doi:10.1029/2008JB005701

Salisbury JB, Rockwell TK, Middleton TJ, Hudnut KW (2012) LiDAR and field observations of slip distribution for the most recent surface ruptures along the Central San Jacinto Fault. Bull Seismol Soc Am 102(2):598–619. doi:10.1785/0120110068

Sammis CG, Rosakis AJ, Bhat HS (2009) Effects of off-fault damage on earthquake rupture propagation: experimental studies. Pure appl Geophys 166:1629–1648. doi:10.1007/s00024-009-0512-3

Savage HM, Brodsky E (2011) Collateral damage: the evolution with displacement of fracture distribution and secondary fault strands in fault damage zones. J Geophys Res. doi:10.1029/2010JB007665

Schmandt B, Clayton RW (2013) Analysis of teleseismic P waves with a 5200-station array in Long Beach, California: evidence for an abrupt boundary to Inner Borderland rifting. J Geophys Res 118:5320–5338. doi:10.1002/jgrb.50370

Scholz CH (1990) The mechanics of earthquakes and faulting. Cambridge University Press, New York

Schulz SE, Evans JP (1998) Spatial variability in microscopic deformation and composition of the Punchbowl fault, southern California: implications for mechanisms, fluid-rock interaction, and fault morphology. Tectonophysics 295:223–244

Schulz SE, Evans JP (2000) Mesoscopic structure of the Punchbowl Fault, Southern California and the geologic and geophysical structure of active strike-slip faults. J Struct Geol 22:913–930

Shapiro NM, Campillo M, Stehly L, Ritzwoller MH (2005) High-resolution surface-wave tomography from ambient seismic noise. Science 307:1615–1618. doi:10.1126/science.1108339

Sieh K, Jones L, Hauksson E, Hudnut K, Eberhart-Phillips D, Heaton T, Hough S, Hutton K, Kanamori H, Lilje A, Lindvall S, McGill SF, Mori J, Rubin C, Spotila JA, Stock J, Thio HK, Treiman J, Wernicke B, Zachariasen J (1993) Near-field investigations of the Landers earthquake sequence. Science 260(5105):171–176

Smith SAF, Bistacchi A, Mitchell TM, Mittempergher S, Toro GD (2013) The structure of an exhumed intraplate seismogenic fault in crystalline basement. Tectonophysics 599:29–44. doi:10.1016/j.tecto.2013.03.031

Stierman DJ (1984) Geophysical and geological evidence for fracturing, water circulation, and chemical alteration in granitic rocks adjacent to major strike-slip faults. J Geophys Res 89:5849–5857

Sutherland R et al (2012) Drilling reveals fluid control on architecture and rupture of the Alpine fault, New Zealand. Geology 40(12):1143–1146. doi:10.1130/G33614.1

Ujiie K , Tanaka H, Saito T, Tsutsumi A, Mori JJ, Kameda J, Brodsky EE, Chester FM, Eguchi N, Toczko S; Expedition 343 and 343T Scientists (2013) Low coseismic shear stress on the Tohoku-Oki megathrust determined from laboratory experiments. Science 342(6163):1211–1214

Vidale JE, Li YG (2003) Damage to the shallow Landers fault from the nearby Hector Mine earthquake. Nature 421:524–526

Waldhauser F, Ellsworth WL (2002) Fault structure and mechanics of the Hayward fault, California, from double-difference earthquake locations. J Geophys Res 107:2054

Wang CY, Rui F, Yao Z, Shi X (1986) Gravity anomaly and density structure of the San Andreas fault zone. Pure appl Geophys 124:127–140

Wang B, Ge H, Yang W, Wang W, Wang B, Wu G, Su Y (2012) Transmitting seismic station monitors fault zone at depth. EOS Trans AGU 93(5):49–50

Wang B, Yang W, Wang W, Wang H, Zheng L, Wei B, Zhang W, Yuan S (2013) Monitoring crustal variation in Northern Tianshan using large-volume air guns. Chinese Geophysical Society Annual Meeting, Kunming

Wibberley CAJ, Yielding G, Toro GD (2008) Recent advances in the understanding of fault zone internal structure: a review. In: Structure of fault zones: implications for mechanical and fluid-flow properties, Geological Society of London Special Publication, London, vol. 299, pp 5–33, doi: 10.1144/SP299.2

Wu C, Peng Z, Ben-Zion Y (2009) Non-linearity and temporal changes of fault zone site response associated with strong ground motion. Geophys J Int 176:265–278. doi:10.1111/j.1365-246X.2008.04005.x

Wu J, Hole JA, Snoke JA (2010) Fault zone structure at depth from differential dispersion of seismic guided waves: evidence for a deep waveguide on the San Andreas Fault. Geophys J Int 182:343–354. doi:10.1111/j.1365-246X.2010.04612.x

Xu S, Ben-Zion Y, Ampuero J-P (2012) Properties of inelastic yielding zones generated by in-plane dynamic ruptures: II. Detailed parameter-space study. Geophys J Int 191:1343–1360. doi:10.1111/j.1365-246X.2012.05685.x

Yang H (2010) Study of earthquake fault zone structures by aftershock location and high-frequency waveform modeling, Ph.D. thesis, Saint Louis University, St. Louis

Yang H, Zhu L (2010a) Shallow low-velocity zone of the San Jacinto fault from local earthquake waveform modelling. Geophys J Int 183:421–432. doi:10.1111/j.1365-246X.2010.04744.x

Yang H, Zhu L (2010b) Depth extent of low-velocity fault zones. Eos Trans AGU 91(52), Fall Meet. Suppl., T33B-2250

Yang H, Zhu L, Chu R (2009) Fault-plane determination of the 18 April 2008 Mt. Carmel, Illinois, earthquake by detecting and relocating aftershocks. Bull Seismol Soc Am 99(6):3413–3420. doi:10.1785/0120090038

Yang H, Zhu L, Cochran ES (2011) Seismic structures of the Calico fault zone inferred from local earthquake travel time modelling. Geophys J Int 186:760–770. doi:10.1111/j.1365-246X.2011.05055.x

Yang H, Liu Y, Lin J (2012) Effects of subducted seamounts on megathrust earthquake nucleation and rupture propagation. Geophys Res Lett. doi:10.1029/2012GL053892

Yang H, Liu Y, Lin J (2013) Geometrical effects of a subducted seamount on stopping megathrust ruptures. Geophys Res Lett 40:2011–2016. doi:10.1002/grl.50298

Yang H, Li Z, Peng Z, Ben-Zion Y, Vernon F (2014) Low velocity zones along the San Jacinto Fault, Southern California, from body waves recorded in dense linear arrays. J Geophys Res. doi:10.1002/2014JB011548

Yang W, Peng Z, Wang B, Li Z, Yuan S (2015) Velocity contrast along the rupture zone of the 2010 M_W 6.9 Yushu, China earthquake from systematic analysis of fault zone head waves. Earth Planet Sci Lett 416:91–97. doi:10.1016/j.epsl.2015.01.043

Yao H, van der Hilst RD, de Hoop MV (2006) Surface-wave array tomography in SE Tibet from ambient seismic noise and two-station analysis—I. Phase velocity maps. Geophys J Int 166:732–744. doi:10.1111/j.1365-246X.2006.03028.x

Zhang J, Gerstoft P (2014) Local-scale cross-correlation of seismic noise from the Calico fault experiment. Earthq Sci 27:1–8. doi:10.1007/s11589-014-0074-z

Zhao P, Peng Z (2008) Velocity contrast along the Calaveras fault from analysis of fault zone head waves generated by repeating earthquakes. Geophys Res Lett. doi:10.1029/2007GL031810

Zigone D, Ben-Zion Y, Campillo M, Roux P (2014) Seismic tomography of the Southern California plate boundary region from noise-based Rayleigh and Love waves. Pure APPL Geophys. doi:10.1007/s00024-014-0872-1